INTERNATIONAL JOURNAL FOR NUMERICAL METHODS IN FLUIDS
Int. J. Numer. Meth. Fluids **30**: 1–18 (1999)

NUMERICAL SIMULATION OF THE FILM CASTING PROCESS

D. SILAGY[a], Y. DEMAY[b] AND J.F AGASSANT[a,*]

[a] *Centre de Mise en Forme des Matériaux, UMR CNRS 7635, École des Mines de Paris, BP 207, 06904 Sophia Antipolis Cedex, France*
[b] *Institut Non Linéaire de Nice, UMR CNRS 129, 1361 route des Lucioles, 06560 Valbonne, France*

SUMMARY

The film casting process is widely used to produce polymer film: a molten polymer is extruded through a flat die, then stretched in air and cooled on a chill roll. This study is devoted to the extensional flow between the die and the chill roll. The film shows a lateral neck-in as well as an inhomogeneous decrease of the thickness. An isothermal and Newtonian membrane model, constituted of an elastic-like equation for velocity coupled to a transport equation for thickness and a free surface computation, is used. These equations are solved via the finite element method (continuous Galerkin for velocity and discontinuous Galerkin for thickness). Both tracking and capturing strategies are used to determine the position of the free surface (lateral neck-in). The influence of the processing parameters (Draw ratio and Aspect ratio) on the film geometry is first determined. The onset of the Draw Resonance instability is then studied through the dynamic response of the process to small perturbations. A critical curve splitting the processing conditions into a stable and an unstable zone is derived. It is shown, consistently, with results of a 1D model, that an increase of the air-gap between the die and the roll improves the stability of the process. Numerical results concerning periodic fluctuations of the flow in unstable conditions are compared with previous experimental results. Copyright © 1999 John Wiley & Sons, Ltd.

KEY WORDS: film casting process; numerical simulation; stability

1. INTRODUCTION

The cast film process is used to produce industrially synthetic film. A molten polymer (for example a low density polyethylene) is extruded through a flat die (for example with a 1 mm opening and a 1 m width), then stretched in air for a short distance (for example 15 cm) and finally cooled down on a chill roll (see Figure 1). Then, in most cases, this film (called primary film) is subjected to other processes, such as biaxial orientation, thermoforming, or coating on a substrate.

The flow between die and chill roll is mostly elongational. A first aspect of interest is the film geometry between the flat die and the chill roll. The film shows a lateral neck-in as well as an inhomogeneous decrease of the thickness. The formation of edge beads surrounding a central area of constant thickness is generally called the dog bone defect. These edge beads

* Correspondence to: Centre de Mise en Forme des Matériaux, UMR CNRS 7635, École des Mines de Paris, BP 207-06904, Sophia Antipolis Cedex, France.

CCC 0271–2091/99/090001–18$17.50

Received 11 November 1996
Revised 1 April 1998

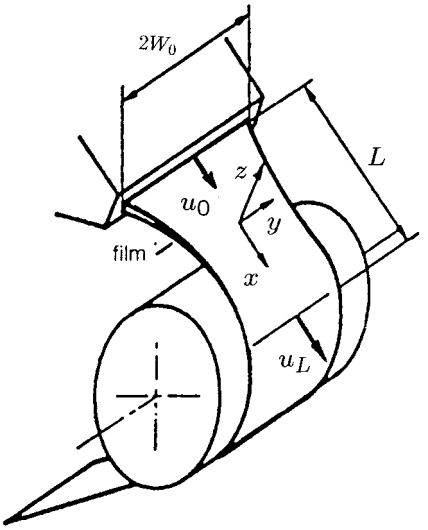

Figure 1. Sketch of the film casting process.

have to be trimmed. The second aspect concerns the stability of the film. Beyond a critical speed of the chill roll, two types of problems may occur. In some cases, a drawing instability known as Draw Resonance and characterized by periodic fluctuations of thickness and width of the film may appear. This instability (close to the one encountered in the fibre spinning process) has been studied both theoretically and experimentally using a 1D model. The reader is referred to [1] for a bibliography and the description of a 1D model (denoted as 1D model in the following) taking into account both width and thickness time fluctuations. In other cases, film breakage is observed and this is generally related to the viscoelastic behaviour of the molten polymer.

In this process, the width of the film as well as the stretching distance are several orders of magnitude larger than the film thickness. Consequently, membrane (2D) models giving a realistic prediction of the dog bone defect have been developed by d'Halewyn *et al.* [2] for a Newtonian fluid and by Debbaut *et al.* [3] for a viscoelastic fluid. These studies are stationary and consequently don't deal with onset of Draw Resonance.

In this paper we develop a Newtonian, isothermal time-dependent membrane model (also denoted as 2D model in the following). The Newtonian hypothesis is relevant for poorly elastic polymers such as some linear low density polyethylenes. The second hypothesis is justified by earlier studies taking into account heat transfer (Cotto *et al.* [4], Barq *et al.* [5]) and showing that the temperature decrease between the die and the roll remains limited. Both tracking and capturing strategies are tested for the computation of the free surface in stationary conditions. The first method uses deformations of an initial mesh whereas the second one uses a fictitious fluid of low viscosity surrounding the polymer film. This last method is used to study the dynamic response of the process to small perturbations. These results are compared to those of the 1D model described in [1].

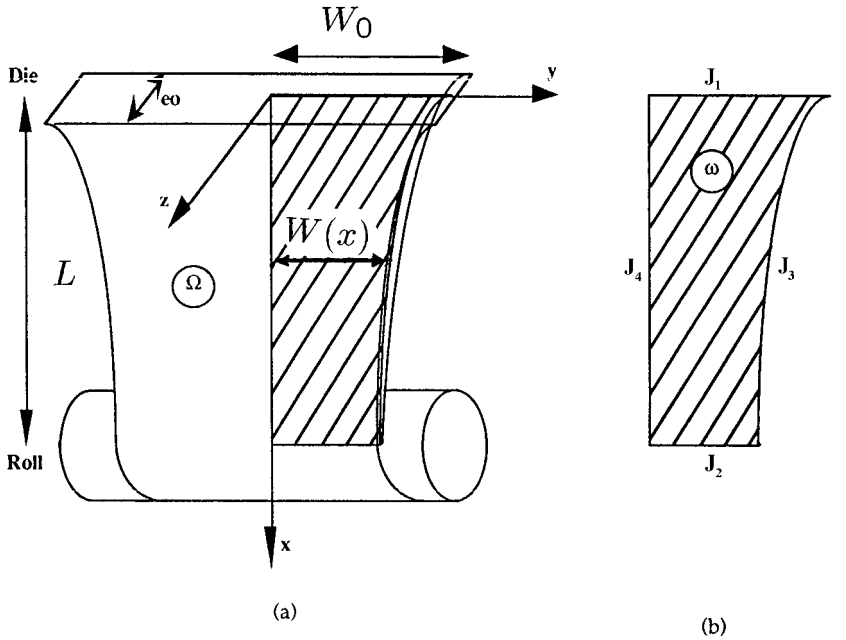

Figure 2. (a) The half flow domain Ω; (b) the half mean surface ω.

2. THE MEMBRANE MODEL

2.1. Kinematic and rate of strain tensor

For the sake of simplicity, we consider that the mean surface of the film is in the plane $z = 0$ (see Figure 2a for the definition of the axes). Let us note L the stretching distance, $W(x)$ the half width (W_0 the half initial width) and $e(x, y)$ the thickness of the film (e_0 the thickness of the die at exit). The key point is that e_0 is small compared to the other dimensions W_0 and L ($L \sim W_0$ and $e_0 \ll W_0$). A first important parameter of the problem is the aspect ratio defined as $A = L/W_0$. The membrane model [2,3] is based on an expansion, classic in shell and membrane theory, according to the small parameter e_0/L. It leads to a system of partial differential equations on the half mean surface ω of the film (see Figure 2b):

$$\omega = \{(x, y)/0 \leq x \leq L, \quad 0 \leq y \leq W(x)\}.$$

Let us note $\mathbf{U} = (u, v, w)$ the velocity field on the half flow domain Ω:

$$\Omega = \left\{(x, y, z)/(x, y) \in \omega / -\frac{1}{2}e(x, y) \leq z \leq \frac{1}{2}e(x, y)\right\}.$$

Components u and v are weakly varying through the thickness and component w is small compared to u and v. As $w(x, y, 0) = 0$, kinematic on $z = 0$ is reduced to a two components velocity field $\tilde{U} = (\tilde{u}, \tilde{v})$ on ω defined by $\tilde{u}(x, y) = u(x, y, 0)$ and $\tilde{v}(x, y) = v(x, y, 0)$. Assuming that the polymer is incompressible leads to:

$$w(x, y, z) \sim z\frac{\partial w}{\partial z}(x, y, 0) = -z\left(\frac{\partial \tilde{u}}{\partial x} + \frac{\partial \tilde{v}}{\partial z}\right). \tag{1}$$

Hence we have, for $z = 0$:

$$[\dot{\epsilon}] = \begin{bmatrix} [\tilde{\epsilon}] & 0 \\ 0 & -\left(\dfrac{\partial \tilde{u}}{\partial x} + \dfrac{\partial \tilde{v}}{\partial y}\right) \end{bmatrix}$$

with

$$[\tilde{\epsilon}] = \begin{bmatrix} \dfrac{\partial \tilde{u}}{\partial x} & \dfrac{1}{2}\left(\dfrac{\partial \tilde{u}}{\partial y} + \dfrac{\partial \tilde{v}}{\partial x}\right) \\ \dfrac{1}{2}\left(\dfrac{\partial \tilde{u}}{\partial y} + \dfrac{\partial \tilde{v}}{\partial x}\right) & \dfrac{\partial \tilde{v}}{\partial x} \end{bmatrix}.$$

More generally (for $z \neq 0$), shear terms $\dot{\epsilon}_{xz}$ and $\dot{\epsilon}_{yz}$ are small compared to in-plane terms $\dot{\epsilon}_{xx}$, $\dot{\epsilon}_{xy}$ and $\dot{\epsilon}_{yy}$. It can be proved using (1) and symmetry according to plane $z = 0$. Denoting u_0 the mid-velocity component in the x-direction at die exit, we have:

$$\dot{\epsilon}_{xz} \sim e_0 \frac{u_0}{L^2}; \quad \dot{\epsilon}_{xy} \sim \frac{u_0}{W_0}$$

and hence

$$\frac{\dot{\epsilon}_{xz}}{\dot{\epsilon}_{xy}} \sim \frac{w_0 e_0}{L^2}$$

where the order of magnitude is 10^{-2} for classical dimensions of the process.

2.2. The stress balance equation

Assuming a Newtonian behaviour, the stress tensor σ and the hydrostatic pressure p are related to the rate of strain tensor $\dot{\epsilon}$ by:

$$[\sigma] = 2\eta[\dot{\epsilon}] - p\ [\mathbf{Id}_3].$$

The equilibrium free surface condition on upper and lower free surfaces of the film ($z = \pm\frac{1}{2}\, e(x, y)$) leads, identifying the normal to the film surface to the z axis, to $\sigma_{zz} = 0$ and hence:

$$[\sigma] = \begin{bmatrix} [\tilde{\sigma}] & 0 \\ 0 & 0 \end{bmatrix} \text{ with } [\tilde{\sigma}] = 2\eta[\tilde{\epsilon}] + 2\eta\left(\frac{\partial \tilde{u}}{\partial x} + \frac{\partial \tilde{v}}{\partial y}\right)[\mathbf{Id}_2]. \tag{2}$$

Integrating the balance equation through the thickness, one obtains the equilibrium equation on domain ω:

$$\nabla_{x,y} \cdot (e[\tilde{\sigma}]) = 0. \tag{3}$$

2.3. The boundary conditions

The boundary of domain ω is composed of the extrusion line γ_1 ($x = 0$; $0 \leq y \leq W_0$), the free surface γ_3 ($0 \leq x \leq L$; $y = W(x)$), the take-up line γ_2 ($x = L$; $0 \leq y \leq W(L)$) and the symmetry line γ_4 ($0 \leq x \leq L$; $y = 0$) (see Figure 3a). Denoting respectively u_0 and u_L extrusion and roll velocities and $\tilde{n}$ the normal to the edge of the film, we have:

$$(x, y) \in \gamma_1 : \tilde{u} = u_0; \quad \tilde{v} = 0; \tag{4}$$

$$(x, y) \in \gamma_2 : \tilde{u} = u_L; \quad \tilde{v} = 0; \tag{5}$$

$$(x, y) \in \gamma_3 : [\tilde{\sigma}]\tilde{n} = 0; \tag{6}$$

$$(x, y) \in \gamma_4 : \tilde{\sigma}_{x,y} = 0; \quad \tilde{v} = 0. \tag{7}$$

The second important parameter of the problem is the Draw Ratio defined as $\mathrm{DR} = u_L/u_0$ and characterizing the intensity of the stretching.

For given values of the thickness field e, the velocity field is the solution of the elliptic partial differential equations and boundary conditions (2)–(7). This elastic-like system is denoted in the following as Pb1.

As the boundary γ_3 (the edge of the liquid film) is a free surface, one has also to satisfy the kinematic free surface condition:

$$\frac{\partial W}{\partial t} + \tilde{u}\frac{\partial W}{\partial x} - \tilde{v} = 0.$$

For given values of the velocity components $\tilde{u}$ and $\tilde{v}$, the half width of the film W is, in stationary conditions, the solution of the following ordinary differential equation with initial data at $x = 0$ (denoted in the following as Pb2):

$$\tilde{u}\frac{\partial W}{\partial x} = \tilde{v}; \quad W(0) = W_0. \tag{8}$$

2.4. The thickness equation

Integrating the mass conservation equation through the thickness and using the kinematic free surface condition on upper and lower bounds, one obtains:

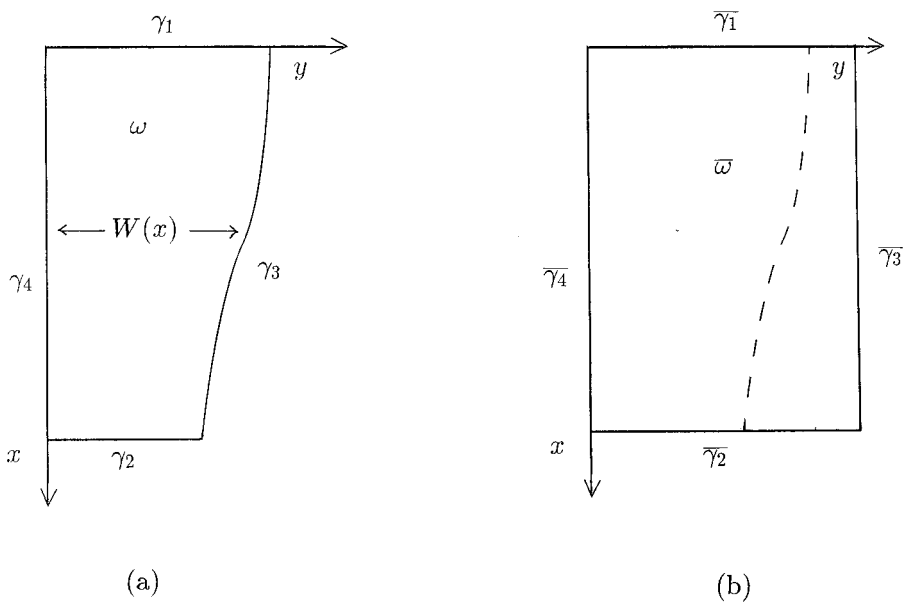

Figure 3. (a) The boundary of domain ω; (b) the boundary of domain $\bar{\omega}$.

$$\frac{\partial e}{\partial t} + \nabla_{x,y} \cdot (e\tilde{U}) = 0. \tag{9}$$

This thickness transport equation has to be solved with the boundary condition:

$$e(0, y) = e_0. \tag{10}$$

In stationary conditions and for given values of the velocity field $\tilde{U}$, thickness e of the film is the solution of the following equations denoted as Pb3 in the following:

$$\nabla_{x,y} \cdot (e\tilde{U}) = 0; \quad e(0, y) = e_0. \tag{11}$$

2.5. The 1D models

The modified problem of the cast film process with constant width is used for testing and initializing in the following. In this case $W(x) = W_0$ and the boundary condition on γ_3 is modified (γ_3 is no more a free surface):

$$(x, y) \in \gamma_3 : \tilde{\sigma}_{x,y} = 0; \quad \tilde{v} = 0. \tag{12}$$

The system of Equations (2)–(5), (7), (11) and (12) has an analytical solution function of x only:

$$e(x, y) = e_0 \left(\frac{u_L}{u_0}\right)^{-x/L}; \qquad \tilde{u}(x, y) = u_0 \left(\frac{u_L}{u_0}\right)^{x/L}; \qquad \tilde{v}(x, y) = 0. \tag{13}$$

This solution, corresponding to small values of the aspect ratio A ($A \sim 0$), is also a classical model for fibre spinning (e denotes in this case the section of the fibre). The stability of this solution has been widely studied. This 1D model of the cast film process was extended for a non-small value of A by assuming that the thickness e is constant on the width [1].

3. COMPUTATION OF THE STATIONARY SOLUTION

As established in the previous section, velocity, thickness and width of the film are, in stationary conditions, solutions of a coupled and non-linear set of equations. It can be split into an elliptic equation for velocity $\tilde{U}$ (Pb1), a free surface problem (Pb2), and a transport equation for the film thickness (Pb3). These problems are solved iteratively and coupled using a fixed point method.

3.1. Computation of the velocity field

For given values of width W and thickness e distributions, the velocity field $\tilde{U}$ solution of Pb1 (Equations (2)–(7)) is computed by using a finite element method. Equation (2) is a particular case of the 2D linear elasticity problem corresponding to Lamé's coefficients $\lambda = 2\eta e$ and $\mu = \eta e$. The solution $\tilde{U}$ minimizes the function F defined as:

$$F(\tilde{U}) = \int\int_{\omega} e[\tilde{\sigma}] : [\tilde{\epsilon}]$$

on the space of velocity fields $\tilde{U}$ satisfying the kinematic boundary conditions. This variational problem is solved by using a continuous-order two finite element method. The flow domain ω is discretized by six nodes and isoparametric triangles.

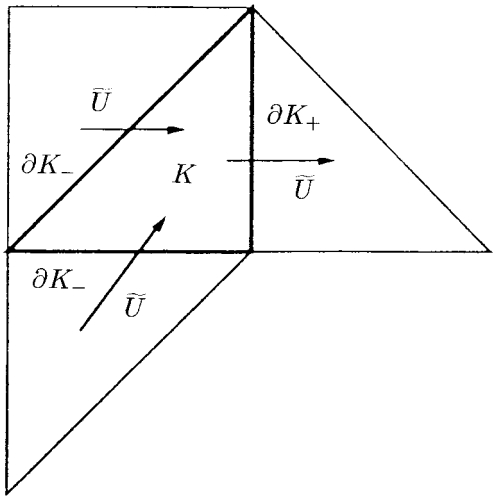

Figure 4. Principle of the discontinuous Galerkin method.

3.2. Computation of the thickness distribution

The thickness distribution e is, for given values of width W and velocity field $\tilde{U}$, the solution of the transport Equation (11) with initial data on $x = 0$ (Pb3).

This problem was solved by d'Halewyn *et al.* [2] using a first-order finite volume method, easy to implement but lacking in numerical precision. We use a discontinuous Galerkin method [6], based on a discontinuous approximation of the film thickness and allowing an element per element treatment of the transport equation. Upwinding is introduced in the Galerkin formulation by considering the thickness jump from the preceding element to the next one. The weak form of the continuity equation on each element K is for any test function ϕ:

$$\iint_K \phi \nabla_{x,y} \cdot (e\tilde{U}) + \int_{\partial K^-} \phi (e - e_{\text{ext}}) \tilde{U} \cdot \tilde{n} = 0. \tag{14}$$

In this formula e_{ext} denotes the thickness on the boundary ∂K^- of inflow elements (see Figure 4). An important feature of the discontinuous Galerkin method is that Equation (14) results in a linear system restricted to each element. The size of this system is equal to the number of unknowns per element (six in our case). It can be easily solved on element K if, thanks to a specific element ordering, e_{ext} has been previously calculated. This is possible because there is no recirculation zone in the film casting process. Resolution starts with elements adjacent to the border γ_1 and follows the flow field $\tilde{U}$ everywhere on the domain ω.

3.3. Computation of the free surface

Two strategies have been tested for the computation of the free surface γ_3. The first one (a tracking strategy) uses the deformation of a rectangular mesh. In this case, free boundary γ_3 is a line joining nodes of the mesh. The second one (a capturing strategy) describes domain ω with a pseudo-concentration function (the thickness in this case) defined in a larger domain. This last method, allowing the use of a constant mesh, will be used for unstationary computations.

3.3.1. Tracking strategy: the deformed mesh method. For a known velocity field, the half width of the film, solution of the ordinary differential Equation (8) is computed by a second-order Runge–Kutta method. The updated mesh of domain ω is obtained as the image of a uniform structured mesh of the rectangular domain $[0, L] \times [0, W_0]$ by the plane transformation ψ:

$$\psi(x, y) = \left(x, y \frac{W(x)}{W_0} \right).$$

3.3.2. Capturing strategy: the fictitious fluid method. It consists of considering a fictitious thickness close to zero outside of ω and solving Equation (9) on a larger domain $\bar{\omega}$ ($\bar{\omega} \supset \omega$). It requires only a single mesh and the free surface is determined *a posteriori*) as an isovalue of the thickness distribution. The discontinuous Galerkin method, presented in the previous section, allows transport of the thickness discontinuity. An element K of the mesh can be in ω, outside of ω, or partly inside and outside. More precisely, let us consider the domain $\bar{\omega} = [0, L] \times [0, W_1]$ with $W_1 \geq W_0$. Boundaries $\bar{\gamma}_k$ of $\bar{\omega}$ are defined in Figure 3b. Let us note $\bar{e}$ the function e extended by zero outside of ω. Then we have on $\bar{\omega}$ (for any continuous extension $\bar{U}$ of $\tilde{U}$):

$$\nabla_{x,y} \cdot (\bar{e}\bar{U}) = \overline{\nabla_{x,y} \cdot (e\tilde{U})} + e\tilde{U} \cdot \tilde{n}\delta_{\gamma_3}.$$

In this equation upperbar denotes extension by zero outside of ω and δ_{γ_3} is the dirac function on γ_3. Hence Equations (8)–(9) are equivalent to the following equation (see Fortin *et al.* [7]):

$$\frac{\partial \bar{e}}{\partial t} + \nabla_{x,y} \cdot (\bar{e}\bar{U}) = 0. \tag{15}$$

For numerical experiments, the thickness e was extended by a small value $\bar{\epsilon} = 10^{-6}$ and Equation (15) was solved by the discontinuous Galerkin method with the following boundary conditions on $\bar{\gamma}_1$ and $\bar{\gamma}_3$: on $\bar{\gamma}_1 : \bar{e}(0, y) = e_0$ for $0 \leq y \leq W_0$ and $\bar{e}(0, y) = \bar{\epsilon}$ for $W_0 < y \leq W_1$, on $\bar{\gamma}_3 : \bar{e}(x, y) = \bar{\epsilon}$. The extended velocity field $\bar{U}$ is computed by solving on domain $\bar{\omega}$:

$$\nabla_{x,y} \cdot (\bar{e}[\bar{\sigma}]) = 0. \tag{16}$$

Let us remark that, as previously, this equation expresses the balance Equation (3) on domain ω and the boundary condition (6) as well. Finally the free surface is computed as the isovalue $e = 10\bar{\epsilon}$.

3.4. The iterative process

Computations of free surface, thickness and velocity are coupled by using a fixed point algorithm. The analytical solution (13) of the constant width film casting (satisfying all equations except boundary conditions (6) and (8)) was used as an initial value.

If a tracking strategy (deformed mesh method) is used, velocity and width are the solution of a free surface problem (for given thicknesses at nodes). The velocity is first computed, then the width. The mesh is therefore deformed and values of the thickness are transported with the mesh. Practically one or two iterations are sufficient. The thickness of the film is then computed by solving Equation (9). New velocity and width distributions are then computed and so on until convergence. Computation is stopped when e/e_0 and W/W_0 vary less than 10^{-3}. Convergence is usually quickly obtained (less than ten free surface iterations and less than five thickness transport iterations). For high values of the Draw Ratio, very large deformations leading to mesh degeneration are applied to the initial mesh. It would require a remeshing technique and careful nodal value computations heavy to implement.

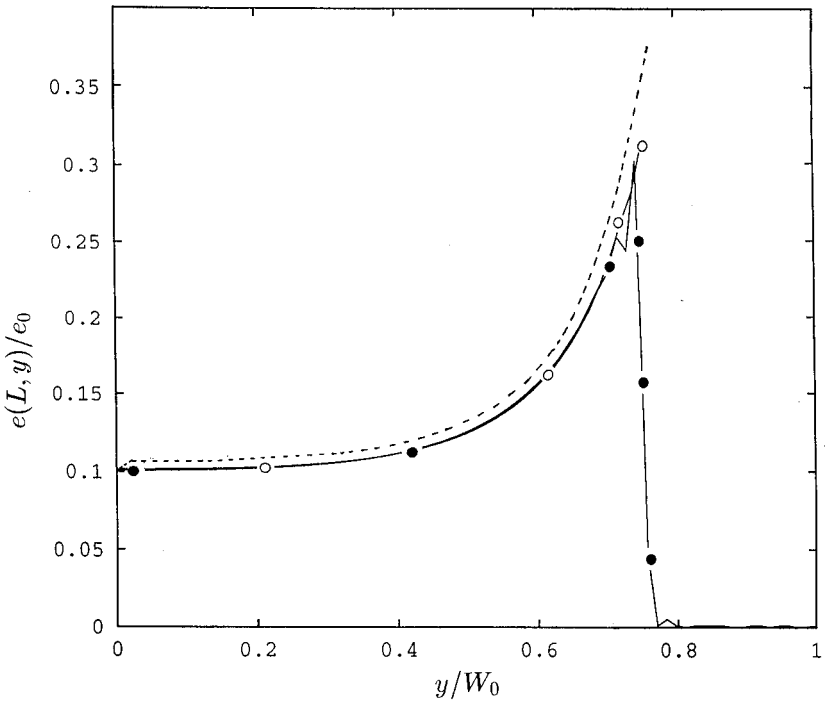

Figure 5. Final thickness profile ($e(L, y)$) obtained for $A = 0.4$ and DR = 10: tracking strategy and finite volume method ([2], - - -); tracking strategy and discontinuous finite element method (○); capturing strategy and discontinuous finite element method (●).

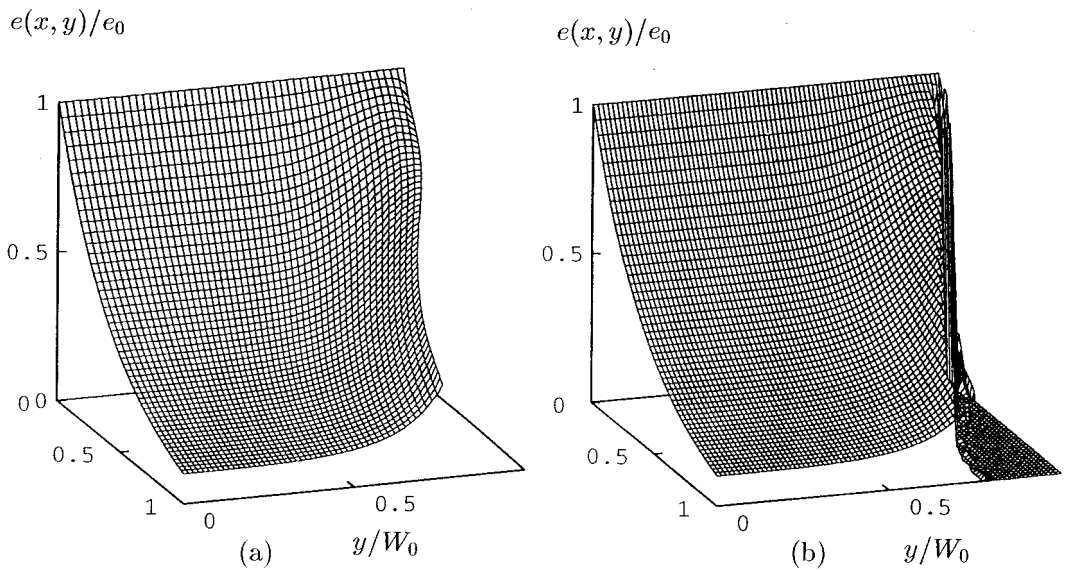

Figure 6. Film shape for DR = 10, $A = 0.4$ computed with a discontinuous finite element method ((a) tracking strategy, (b) capturing strategy).

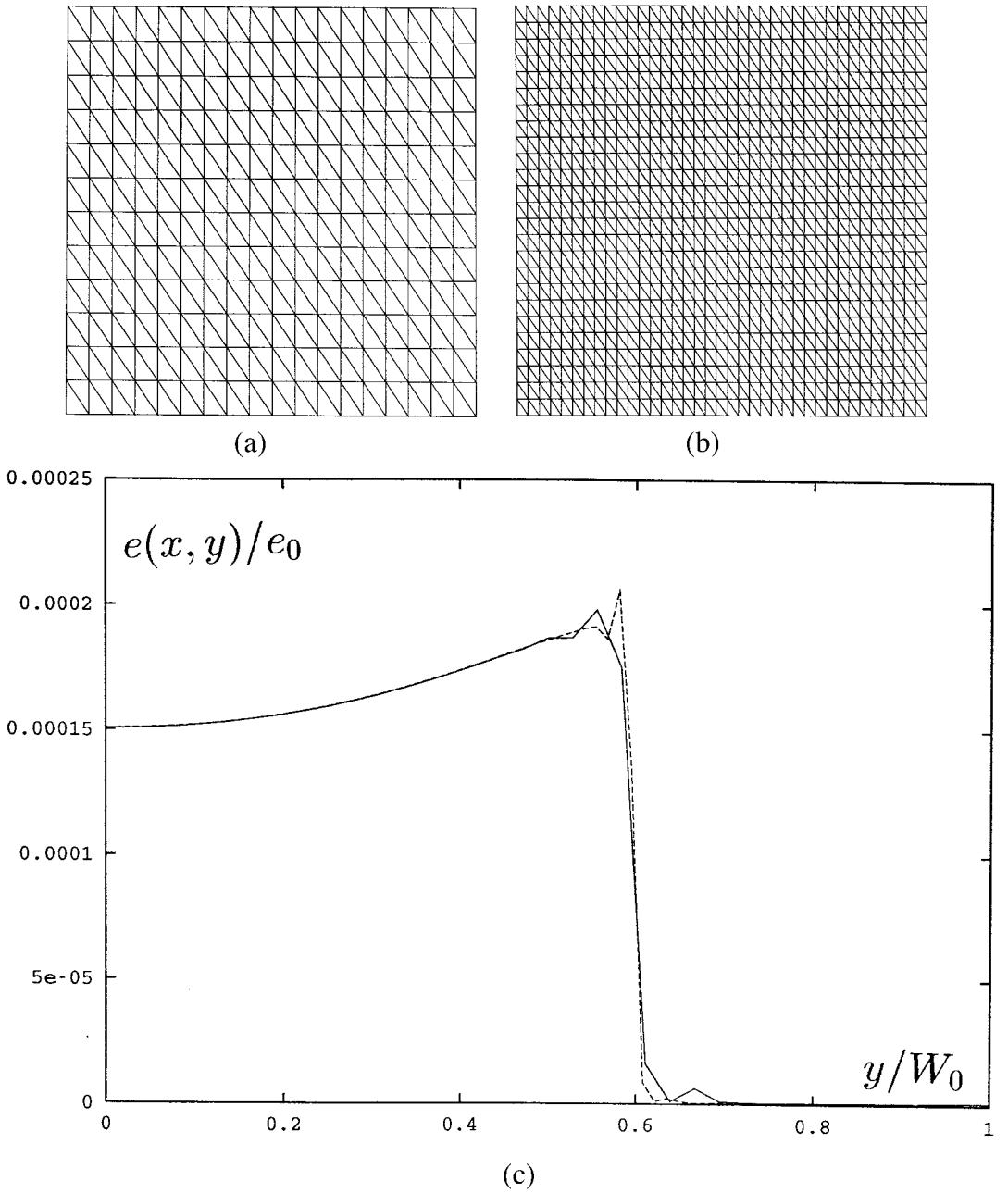

Figure 7. (a) Coarse mesh; (b) refined mesh; (c) final thickness profile $e(L, y)$ for DR = 10, $A = 1$ (capturing strategy) on coarse mesh (—) and refined mesh (- - -).

If a capturing strategy (fixed mesh method) is used, thickness and width are obtained simultaneously from Equation (15). As a consequence, the computation algorithm is largely simplified and convergence is more rapidly achieved. Hence this method, which is easier to implement, is used to solve the time-dependent problem.

4. STATIONARY RESULTS

In this section we first compare the different numerical strategies and we study mesh convergence. Then we compare these 2D results with the previous 1D models of the film casting process.

4.1. Numerical results

Figure 5 plots the final thickness profile ($e(L, y)$) obtained for $A = 0.4$ and $\mathrm{DR} = 10$, respectively, with a tracking strategy and a finite volume method (see d'Halewyn *et al.* [2]), with a tracking strategy and a discontinuous Galerkin method and with a capturing strategy and a discontinuous Galerkin method. These thickness profiles are very close. The discontinuous Galerkin method provides more precise results (without a spurious thickness jump on the symmetry axis). If a capturing strategy is used, small oscillations in the neighbourhood of the edge of the film are a consequence of the transport of discontinuous functions.

Figure 6 plots global film shapes (thickness and width distributions) for $\mathrm{DR} = 10$ and $A = 0.4$ computed with a discontinuous finite element method ((a) tracking strategy, (b) capturing strategy). There is good agreement between these two methods.

Mesh convergence is tested for the capturing strategy for $\mathrm{DR} = 10$ and $A = 1$. The (fixed) coarse and refined meshes are presented in Figure 7a and b. Figure 7c plots the final thickness profile $e(L, y)$ computed using these meshes. Results are equivalent in the central part of the film. The refined mesh will be used for unstationary computations.

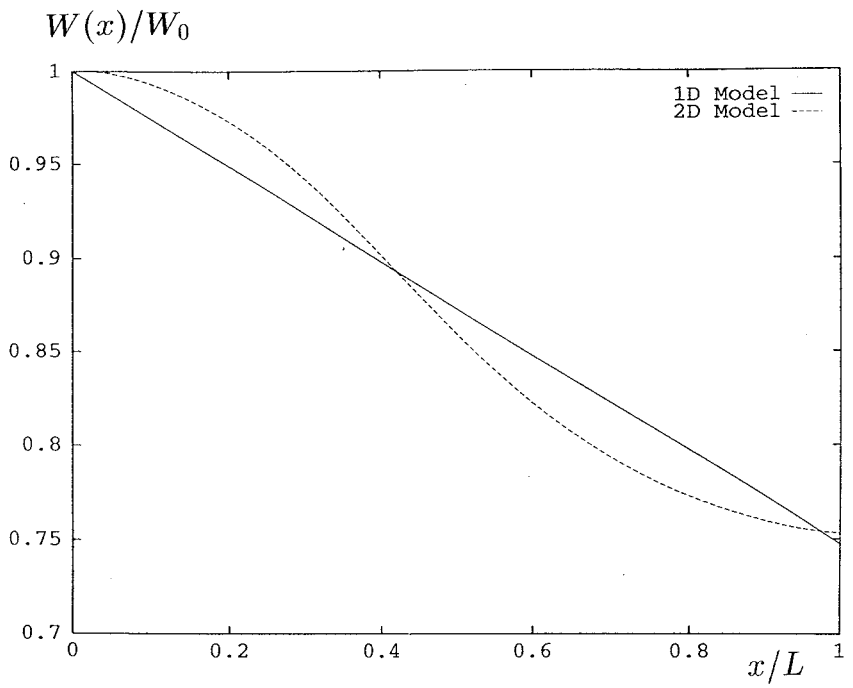

Figure 8. Free surface for $\mathrm{DR} = 10$, $A = 0.4$ and comparison with result of the 1D model.

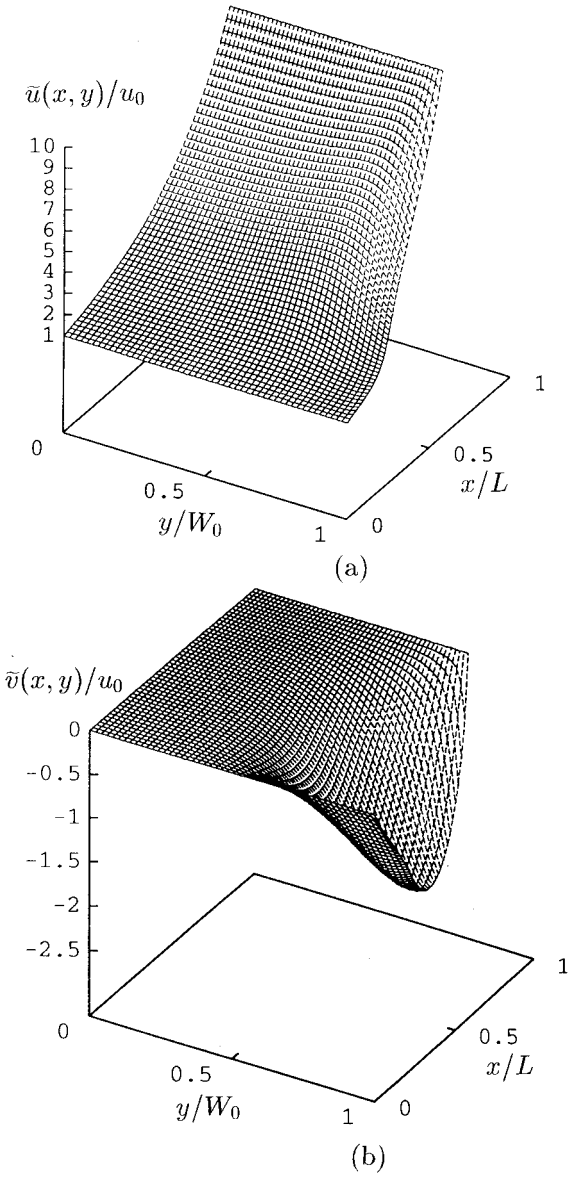

Figure 9. Velocity components profiles: (a) $\tilde{u}$; (b) $\tilde{v}$.

4.2. Comparison with previous works

Figure 8 compares the free surface obtained with this 2D model to the one obtained with a 1D Newtonian model [1]. The 2D free surface is no longer linear between the die and the roll and this is consistent with experiments. Figure 9a and b, presents the distribution of the two components $\tilde{u}$ and $\tilde{v}$ of the velocity field. Two different flow zones are clearly pointed out. Component $\tilde{v}$ is nearly equal to zero between $y = 0$ and $y = \frac{1}{2} W_0$. This means that uniaxial extension occurs in the central part of the film and biaxial extension at the edges of the film.

This is consistent with the mechanical analysis provided by Dobroth *et al.* in [8] explaining the existence of the dog bone defect.

As the thickness of the final film has to be as regular as possible the lateral edge beads are cut and recycled. Figure 10 draws the thickness profile on the chill roll ($e(L, y)$) for DR = 10 and different values of the aspect ratio ($A = 0.2$, 0.4 and 0.8).

5. UNSTATIONARY APPROACH

5.1. The time-dependent scheme

A fully implicit Gear scheme is used for Equation (15):

$$\frac{\partial \bar{e}(t)}{\partial t} = \frac{1}{2\Delta t}(3\bar{e}(t) - 4\bar{e}(t-\Delta t) + \bar{e}(t-2\Delta t)). \tag{17}$$

It is second-order in time and is accurate for the prediction of time-dependent problems. As it requires at time t the knowledge of the thickness at time $t-\Delta t$ and $t-2\Delta t$, the classical Euler scheme was used at the first step:

$$\frac{\partial \bar{e}(t)}{\partial t} = \frac{1}{\Delta t}(\bar{e}(t) - \bar{e}(t-\Delta t)).$$

As Equations (2)–(7) are not modified, it results in few modifications in the discontinuous Galerkin formulation of the fictitious fluid method. The fixed point algorithm is unchanged. A convenient value of the time step Δt is determined in the next section.

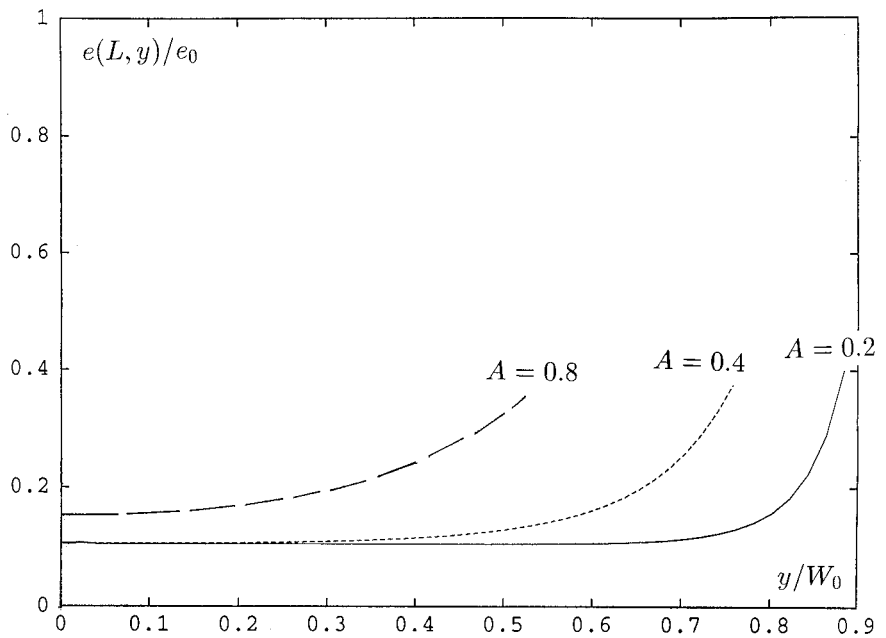

Figure 10. Final thickness profile $e(L, y)$ for DR = 10: $A = 0.2$ (—); $A = 0.4$ (- - -); $A = 0.8$ (– –).

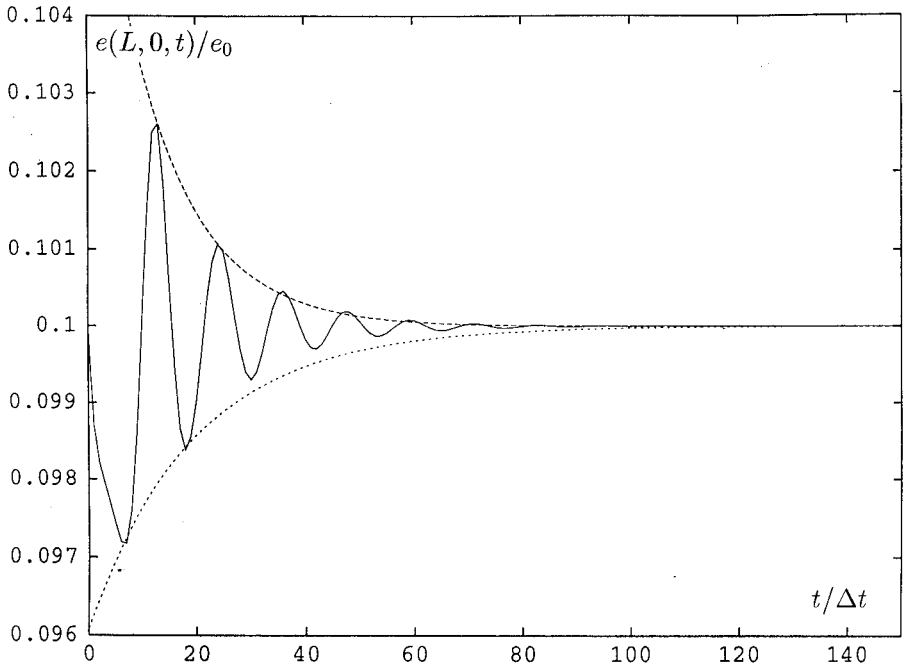

Figure 11. Evolution of the final thickness with time for the constant width cast film process (DR = 10, $A = 0$).

5.2. Time step determination

The stability of the analytic solution (13) of the modified problem presented in section 2.5 has been widely studied (see [1] for references). At a critical Draw Ratio $DR_C = 20.2$ a Hopf bifucation occurs. A pair of complex conjugate eigenvalues $\lambda = \pm i14.06$ cross the imaginary axis and the steady state solution (13) becomes unstable. The linear stability method, used to study the stability of the 1D model, allows to determine very precise values of the dominant eigenvalues and DR_C. By measuring the period of the thickness fluctuations of a time-dependent simulation (Figure 11) in stable conditions ($DR < DR_C$) and fitting the exponential decay, one can estimate real and imaginary parts of the dominant eigenvalues (eigenvalues of greatest real part). Those estimates can be compared with the very precise results of the 1D model for $A = 0$. A time step $\Delta t = 2.5 \times 10^{-3}$, found to give a good agreement (see Table I), is used in the following.

Table I. Eigenvalue for DR = 10, $A = 0$ and comparison with the result of the 1D model

Δt	$Re(\lambda)$	$Im(\lambda)$
1.0×10^{-3}	−1.62	11.42
2.5×10^{-3}	−1.45	11.57
5.0×10^{-3}	−1.55	10.77
1D model	−1.44	11.86

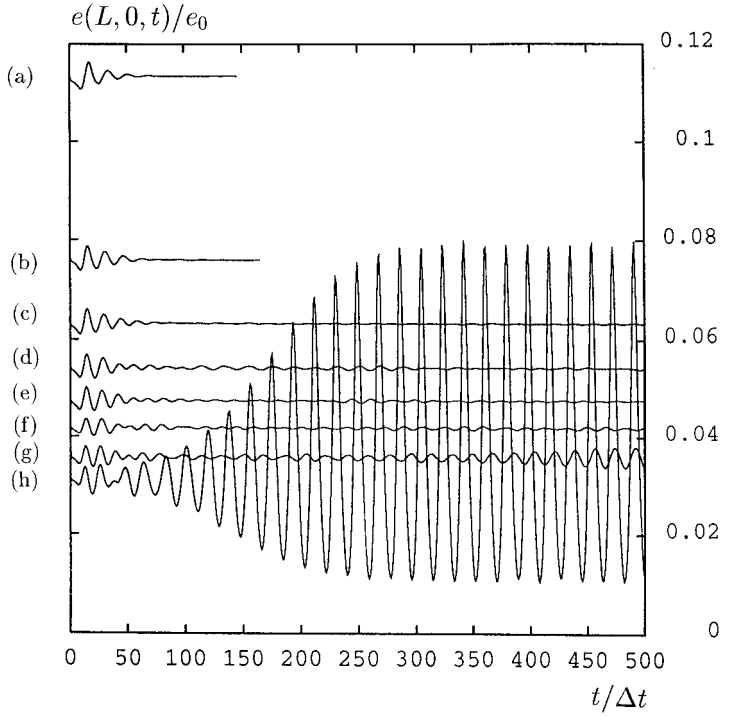

Figure 12. Evolution of the final thickness in the middle part of the film with time for $A = 0.6$ and different values of DR: (a) DR = 10; (b) DR = 15; (c) DR = 18; (d) DR = 21; (e) DR = 24; (f) DR = 27; (g) DR = 31.5; (h) DR = 36.

5.3. The onset of Draw Resonance instability

The 2D model is used to study the response of the system to an imposed perturbation. If this perturbation vanishes with time, it means that the process is stable. Figure 12 plots the evolution with time of the final thickness in the central part of the film ($x = L$, $y = 0$) for $A = 0.6$ and for different values of the Draw Ratio. For low values of the Draw Ratio ($10 \leq \mathrm{DR} \leq 24$), the perturbation decreases with time more and more slowly as DR increases. For $\mathrm{DR} = 31.5$ and $\mathrm{DR} = 36$, the evolution of the thickness with time tends to sustained periodic oscillations. This instability, known as draw resonance, occurs above a critical Draw Ratio denoted $\mathrm{DR_C}$. For $A = 0.6$, we have $27 \leq \mathrm{DR_C} \leq 31.5$. The corresponding value for the 1D model (obtained more precisely) is $\mathrm{DR_C} = 27.3$.

5.4. Critical curves

The critical curve is determined by studying the influence of A on the critical Draw Ratio. For the 2D model, the critical Draw Ratio is delimited between stable and unstable values of the Draw Ratio corresponding to the vanishing or non-vanishing behaviour of perturbations. It leads to an estimated critical curve plot which is compared to the (more precise) critical curve of the 1D model in Figure 13. The 2D model predicts that the aspect ratio A has a stabilizing effect on the process and this effect is more pronounced than with the 1D model. It means that the dog bone defect stabilizes the process. It leads to a maximum critical Draw Ratio $\mathrm{DR_C} = 45$ for an aspect ratio of 1. It should be noted that for $A > 1.2$, the 2D critical Draw Ratio is smaller than the 1D one.

6. COMPARISON WITH EXPERIMENTAL RESULTS

In this section, we compare our results with experiments of Barq *et al.* [9] for the polyester film extrusion process. They pointed out an interesting coupling between width and thickness fluctuations. The film thickness is maximum in the middle when the width is minimum. There is also a phase opposition for thickness oscillations in the middle and on the edge of the film.

Because of its low elasticity level, polyester can be considered as Newtonian. We test our unstationary approach for the same operating conditions ($A = 0.44$ and $\mathrm{DR} = 28.4$). Our model predicts that the process is nearly stable ($\mathrm{DR_C} \sim 28.5$), whereas Barq *et al.* mention an unstable situation. It means that the real critical Draw Ratio is smaller than the one predicted by our model. This can be explained by the fact that the (3D) extrudate swell phenomenon at the die exit is not taken into account. It is consistent with the recent work of Souli *et al.* [10] showing that considering die swell in the constant width cast film process leads to the prediction of smaller critical Draw Ratios. Following these authors, it can be considered that swelling at flat die exit induces a 18% reduction of the extrusion velocity and hence an 18% increase of the critical Draw Ratio. These considerations lead to a real Draw Ratio $\mathrm{DR} \sim 33$. Our model predicts in these conditions sustained periodic oscillations of width, thickness in the central part and thickness on the edge of the film as shown in Figure 14. It shows clearly that, in agreement with the experimental results of Barq *et al.*, width and thickness on the edge of the film are in phase opposition with thickness in the central part of the film.

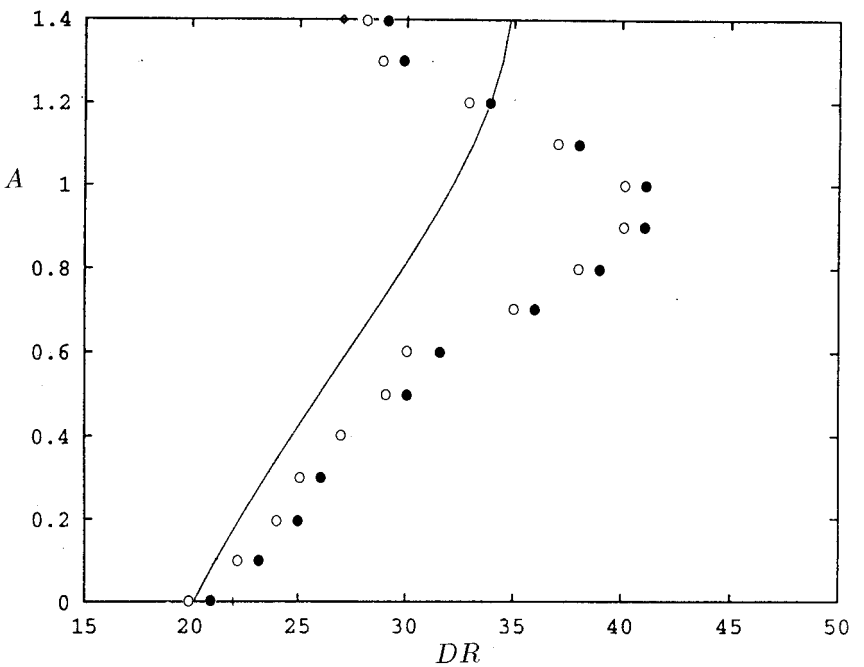

Figure 13. Stability results and comparison with the 1D model: 2D stable (○); 2D unstable (●); 1D critical curve (—).

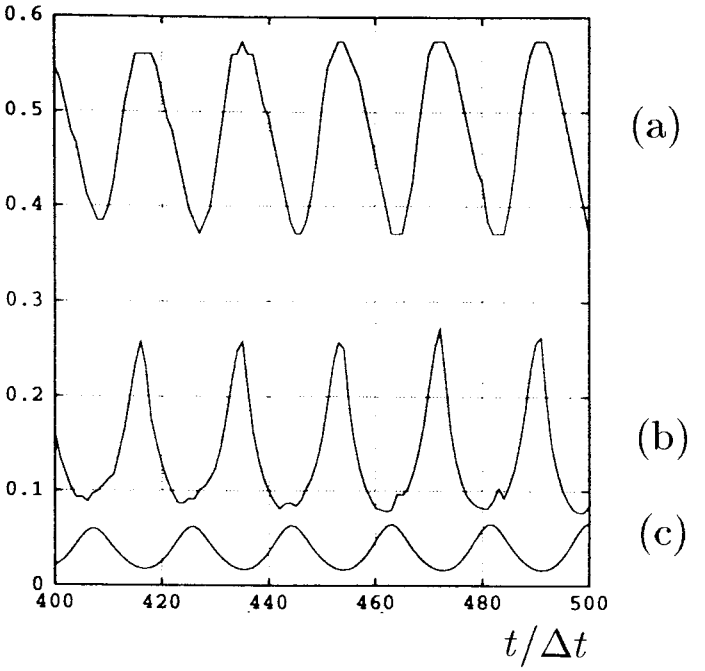

Figure 14. Dimensionless width, edge thickness and central thickness fluctuations for DR = 33, $A = 0.6$: (a) $W(L, t)/W_0$; (b) $e(L, W(L, t), t)/e_0$; (c) $e(L, 0, t)/e_0$.

7. CONCLUSIONS

This 2D Newtonian isothermal model of the film casting process in both stationary and unstationary conditions leads to a non-linear coupled problem involving a free surface elliptic system for velocity on the mean surface and a transport equation for the thickness of the film. Velocity and thickness are separately computed (using, respectively, continuous and discontinuous finite element methods) and coupled with a fixed point algorithm.

Concerning the computation of the steady free surface, two different strategies were considered. The first one, already used in [2], is a tracking strategy considering nodes at the free surface as unknowns. The second one (a capturing strategy) introduces a fictitious fluid (of very small thickness) in the neighbourhood of the film. The free surface is, in this case, determined as the interface between the polymer fluid and the fictitious fluid. Both approaches give consistent predictions of the so called dog bone defect with a reasonable computation time. From a practical point of view, the fictitious fluid method is easier to implement and used to study the stability of the process. The stationary results show that the process parameters (DR and A) have a marked influence on the final section of the film.

The unstationary approach enables study of the influence of these parameters on the onset of the draw resonance phenomenon. The critical curve shows that, consistent with the 1D model predictions, the aspect ratio A has a stabilizing effect on the process (the instability phenomenon can be postponed by increasing the aspect ratio). It was also found that the phase shift between width and thickness fluctuations is consistent with the experimental observations of Barq. *et al.*

ACKNOWLEDGMENTS

The authors gratefully acknowledge the Machelen Chemical Technology Center (Machelen, Belgium) of the Exxon Chemical Europe Company for financial support and more particularly François Chambon for fruitful discussions.

REFERENCES

1. D. Silagy, Y. Demay and J.F. Agassant, 'Etude de la stabilité de l'étirage d'un fluide Newtonien', *C. R. Acad. Sci. Paris II*, **322**, 283–289 (1996).
2. S. d'Halewyn, Y. Demay and J.F. Agassant, 'Numerical simulation of the cast film process', *Polym. Eng. Sci.*, **30**, 335–340 (1990).
3. B. Debbaut and J.M. Marchal, 'Viscoelastic effects in film casting', *Z. Angew Math. Phys.*, **46**(special issue), 679–698 (1995).
4. D. Cotto, P. Saillard, J.F. Agassant and J.M. Haudin, 'Influence of processing conditions on two step biaxial stretching of polypropylene films', in J.C. Siferis and P.S. Theocaris (eds.), *Interrelations between Processing, Structure and Properties of Polymeric Materials*, Elsevier, Amsterdam, 1984.
5. P. Barq, J.M. Haudin and J.F. Agassant, 'Isothermal and anisothermal models for cast film extrusion', *Intern. Polym. Process.*, **VII**, 334 (1992).
6. P. Lesaint and P.A. Raviart, 'On a finite element method for solving the neutron transport equations', in C. de Boor (ed.), *Mathematical Aspect of Finite Elements in Partial Differential Equations*, Academic Press, New York, 1974, p. 89.
7. A. Fortin, P. Carrier and Y. Demay, 'Numerical simulation of coextrusion and film casting', *Int. J. Numer. Methods Fluids*, **20**, 31–57 (1994).
8. T. Dobroth and L. Erwin, 'Causes of edge beads in cast films', *Polym. Eng. Sci.*, **26**, 462 (1986).
9. P. Barq, J.M. Haudin, J.F. Agassant, H. Roth and P. Bourgin, 'Instability phenomena in film casting process', *Intern. Polym. Process.*, **V**(4), 264 (1990).
10. M. Souli, Y. Demay and M. Habbal, 'Finite element study of the Draw Resonance instability', *Eur. J. Mech. B/Fluids*, **12**, 1–13 (1993).

